Mathematical Biosciences and Engineering

MBE, 20(2): 3944–3969.
DOI: 10.3934/mbe.2023184
Received: 17 November 2022
Revised: 03 December 2022
Accepted: 06 December 2022
Published: 14 December 2022

http://www.aimspress.com/journal/MBE

*Research article*

# Spatiotemporal patterns and collective dynamics of bi-layer coupled Izhikevich neural networks with multi-area channels

**Guowei Wang[1] and Yan Fu[2,*]**

[1] School of Education, Nanchang Institute of Science and Technology, Nanchang 330108, China
[2] School of Mathematics and Computer Science, Yuzhang Normal University, Nanchang 330108, China

* **Correspondence:** Email: fuyan@yuznu.edu.cn.

**Abstract:** The firing behavior and bifurcation of different types of Izhikevich neurons are analyzed firstly through numerical simulation. Then, a bi-layer neural network driven by random boundary is constructed by means of system simulation, in which each layer is a matrix network composed of 200 × 200 Izhikevich neurons, and the bi-layer neural network is connected by multi-area channels. Finally, the emergence and disappearance of spiral wave in matrix neural network are investigated, and the synchronization property of neural network is discussed. Obtained results show that random boundary can induce spiral waves under appropriate conditions, and it is clear that the emergence and disappearance of spiral wave can be observed only when the matrix neural network is constructed by regular spiking Izhikevich neurons, while it cannot be observed in neural networks constructed by other modes such as fast spiking, chattering and intrinsically bursting. Further research shows that the variation of synchronization factor with coupling strength between adjacent neurons shows an inverse bell-like curve in the form of "inverse stochastic resonance", but the variation of synchronization factor with coupling strength of inter-layer channels is a curve that is approximately monotonically decreasing. More importantly, it is found that lower synchronicity is helpful to develop spatiotemporal patterns. These results enable people to further understand the collective dynamics of neural networks under random conditions.

**Keywords:** spatiotemporal patterns; spiral waves; Izhikevich neurons; stochastic boundaries; matrix networks; mode transformation

## 1. Introduction

As an important branch in the field of nonlinear dynamics, the research scope of pattern dynamics involves biology, physics, mathematics, chemistry, medicine, astronomy and other disciplines, and the research in various interdiscipline has become a hot spot for researchers [1]. Pattern formation is a kind of non-uniform macro structure with certain regularity in time or space, which extensively exists in nature, such as pattern formed by self-organization in organic polymers, crystal structure in inorganic chemistry, stripes on the surface of animal fur, streak clouds in the sky, etc [2]. From the thermodynamic point of view, the first two types of patterns are those existing in the thermodynamic equilibrium state, and the last two examples are those generated when leaving the thermodynamic equilibrium state [3]. Pattern dynamics is an important branch in the field of nonlinear science [4]. Its research purpose is to explore the basic laws of pattern formation and evolution, which are common among various systems in the objective world and have universal guiding significance [5]. In recent years, as a group of interconnected basic units, complex dynamic networks have attracted more and more attention in many fields such as social science, biology, mathematics and engineering science [6]. In complex dynamic networks, one of the interesting and remarkable phenomena is to show collective behavior [7]. Collective behavior is an important attribute of complex systems, which means that the whole is greater than the sum of parts [8]. Because complex networks are natural spatiotemporal systems, patterns can be observed in these systems [9]. Spatial patterns, such as target patterns, spiral waves and vortex waves, are examples of patterns that occur in complex systems, such as reaction-diffusion systems and neural networks [10].

Spiral wave is a kind of important non-equilibrium pattern, which reflects the macroscopic structure of nonlinear system with some special laws in time or space, and widely exists in excitable, oscillatory and bistable systems [11]. It's mentioned in many literatures that spiral wave is a traveling wave rotating outward from the spiral center in a two-dimensional excitable medium [12]. Generally speaking, the formation of spiral wave is either the free end generated in the propagation wave or the wave collision generated in the inhomogeneous medium [13]. Many interesting works have been carried out, most of which have been proved to be effective in removing spiral waves and preventing spiral waves from breaking [14]. It's believed that the spiral wave in the heart tissue is harmful, so many schemes have been proposed to inhibit the spiral wave and prevent the spiral wave from breaking [15]. Neural network is a complex dynamic network, which can show many active states of spatial structures, such as spatiotemporal chaos, stochastic resonance, synchronization, chimeric state and spiral wave [16]. Network structure, neural model, even considering disturbance and noise, which are inherent properties of neural network, will affect the formation of patterns [17]. Studying these phenomena can bring new insights into the function of neurons [18,19]. Among the tools for studying neural networks, wave propagation mechanism is one of the most effective mechanisms [20]. Spiral wave is a kind of collective behavior, which exists widely in nature [21]. In fact, spiral wave is a special propagation of nonlinear wave [22]. It rotates around a center (called seed), which determines the wave dynamics [23]. It is very important to study the dynamics of spiral waves, because they have been observed in neocortex and arrhythmia of mammals [24]. It has been proved that both atrial fibrillation and ventricular fibrillation are caused by spiral waves [25]. The spiral seed in the heart fiber rotates more frequently than the natural frequency of the heart, making the heartbeat irregular [26]. Therefore, it can cause fibrous fibrillation [27]. Therefore, modeling and identifying the structures formed by spiral waves can help design methods to eliminate spiral waves and control fibrillation [28].

The combination of chemical, physical, electrical and structural characteristics of neurons makes them highly complex dynamic units [10]. Zhao et al. introduced some recent developments in the

dynamic behavior of complex networks (CNs) and complex networks with multi-weights (CNMWs) under various control methods, and several output synchronization criteria for multiple output coupled complex networks (MOCCNs) were formulated by using the Lyapunov functional method and inequality techniques. [29,30]. One of the best tools to deal with this advanced complexity is to study neural spatiotemporal patterns [31]. The electrophysiological and structural characteristics of neurons in neural networks lead to complex characterization [32,33]. These performances are the driving force behind our biological behavior as human beings [34]. Technically, the firing rhythm of neurons determines the function of the brain [35]. These rhythms mainly include spikes and bursts, or a combination of these two modes [36]. In other words, they help us better understand their functions, although there is little detailed information about their chemical, electrical, morphological and structural properties [37]. In this field, one of the most important models is the spiral model. This pattern can be observed in many chemical, biological, physical and ecological systems [38]. Spirals are unique because they are self-organizing and self-sustaining [10,39]. They can play a regulatory role in a system and change its dynamics [40]. For example, there is experimental evidence that spiral waves are crucial to some ongoing cortical activities, because they act as rhythmic regulators in neural populations [41]. Sleep disorders, seizures and attention deficit hyperactivity disorder are just a few examples [42]. Spiral waves can also cause arrhythmias. They are considered to be the main cause of reentry wave front [43]. Reentry is one of the most prominent types of arrhythmia, which can lead to sudden death [44]. From the perspective of experimental research, spiral waves widely exist in nature, such as the oxidation of carbon monoxide on platinum [45]. Biological experiments found that spiral waves also exist in the cerebral cortex [46]. The appearance of spiral wave is also observed in human cardiac muscle [47]. Using a simple active medium model, Kuklik et al. studied the influence of spatial spreading inhomogeneity of transverse element coupling on spiral wave trajectory [48]. They also used the FitzHugh-Nagumo model of an excitable medium to investigate the effect of the random perturbation of cell coupling on the stability of a spiral wave in 2010 [49]. They believed that electrical cardioversion could lead to one of three outcomes, such as immediate termination of arrhythmic activity, delayed termination or unsuccessful termination, and they propose a model of atrial fibrillation as a coexistence of several spiral waves fixed in an active medium with inhomogeneity [50]. In Kumar and Amita Das's work, molecular dynamics simulation was used to prove the excitation of two-dimensional dusty plasma at the particle level [51]. Kwon et al. clearly demonstrated that the new mechanism can create a period-2 helix by computer simulation of a simple mathematical model describing the dynamics of the spiral wavefront [52]. Lacitignola et al. tested some findings by numerical approximations of the complete model and found interesting scenarios that led to spiral fracture to obtain appropriate changes in system parameters [53]. Studies have shown that researchers studying the firing activity of neurons in the cerebral cortex have also observed patches with spiral waves that are closely related to the information transmission between neurons in the brain's neural network [54]. In experimental studies, researchers have found that cardiac patients can also discharge myocardial tissue cells in spiral waves, and more seriously, spiral wave rupture may cause heart fibrillation, resulting in sudden cardiac death and causing serious consequences [55]. In general, the study of spiral waves has very important practical significance [8].

Little problem has been reported about the spatiotemporal dynamics in neural networks constructed by Izhikevich neurons derived from the modeling of cortical neurons at present [56]. At the same time, considering that Izhikevich neurons have many different types of discharge patterns, people basically only consider them as excitatory or inhibitory neurons to build neural networks when they are used for analysis, but rarely consider the formation and rupture of spiral waves in the neural networks [57]. According to the existing research, the neural network of the cerebral cortex has a 5-

layer structure, so the bi-layer network is the most basic component. Neurons will inevitably connect with other neurons around them, which is actually the channel for information exchange and connection. Under the influence of these complex factors, neural networks will show different synchronization properties and spatiotemporal patterns. Moreover, it is unclear whether the neural networks constructed by different types of Izhikevich neurons can induce spiral waves [58]. In this paper, the matrix neural networks constructed by several different types of Izhikevich neurons under the random boundary conditions are discussed, and the influence of the coupling strength between neurons on spatiotemporal dynamics are investigated. A square neural network driven by random boundary is constructed firstly, and then multiple connection regions are set on the network to connect with the second layer neural network. The first layer generates spiral waves, which are transmitted from multiple regions to the second layer, and then the formation and rupture of spiral waves are observed from the second layer. In order to have a clearer understanding of cortical neural networks, the synchronization of the second layer network is also studied by changing the coupling strength between neurons as well as the inter-layer connection strength, and the change of synchronization factor with the coupling strength between neurons in the second layer also shows very interesting results. The arrangement of the paper is as follows: In Section 2, the Izhikevich neuronal model is introduced and the matrix network is constructed; In Section 3, the numerical simulation results are analyzed; Section 4 summarizes the important research conclusions of the research.

## 2. Models and methods

### *2.1. Izhikevich neuronal model*

To understand how the brain works, people needs to combine experimental studies of the animal and human nervous systems with numerical simulations of large-scale brain models [59]. Eugene M. Izhikevich proposed a neuronal model in 2003 which is computationally simple, but capable of producing the rich firing patterns exhibited by real biological neurons [60]. The Izhikevich neuronal model is biologically as plausible as the Hodgkin-Huxley neural model, and is as computationally efficient as the integrate-and-fire neural model [61]. The reason why we choose Izhikevich neuronal model from various neuronal models is that the main modeling object of this model is cortical and thalamic neurons, which can reproduce all their known neuronal firing behaviors, and has simple structure, rich physiological significance, and high computing efficiency. And more importantly, it is applicable to network simulation. The Izhikevich neuronal model driven by external stimulation currents can be represented as follows

$$\begin{cases} \dfrac{dv}{dt} = 0.04v^2 + 5v + 140 - u + I, \\ \dfrac{du}{dt} = a(bv - u). \end{cases} \tag{1}$$

where $v$ represents the membrane potential of the cerebral cortical neuron, and $u$ represents the recovery variable, both of them are dimensionless variables [62]. Constants $a$ and $b$ are used to control different types of neurons, $I$ is considered as external stimulus current [63].

When the value of neuronal membrane potential is greater than the peak value, that is, if $v > 30$ $mV$, the membrane potential is reset in the following way

$$\begin{cases} v \to c, \\ u \to u + d. \end{cases} \tag{2}$$

where $c$ and $d$ are constants.

Different setting of the constants $a$, $b$, $c$ and $d$ yields several typical models of the Izhikevich neuron with different firing types, for example, regular spiking (RS), fast spiking (FS), Chattering (CH) and intrinsically bursting (IB) [64]. The specific values and corresponding discharge types are given in the table as below.

**Table 1.** Control parameters of neurons with different discharge types.

| Types | $a$ | $b$ | $c$ | $d$ |
|---|---|---|---|---|
| RS | 0.02 | 0.2 | –65 | 8 |
| FS | 0.1 | 0.2 | –65 | 2 |
| CH | 0.02 | 0.2 | –50 | 2 |
| IB | 0.02 | 0.2 | –55 | 4 |

### *2.2. Izhikevich neural network*

In order to study the collective properties and spatiotemporal patterns of neural network, a matrix neural network which contains 200 × 200 nodes is constructed in the first step, and all neurons are evenly placed in each node [65]. A certain neuron is connected to other neurons at four locations, upper, lower, left and right, with connection strength $D$, and the schematic diagram of the connections between neurons is plotted in Figure 1. For the boundary of the matrix neural network, the no-flow boundary condition is considered [66]. The no-flow boundary condition considers that the current value inside the boundary is equal to that outside the boundary, that is, the current value outside the boundary is the same as the value setting inside the boundary, thus the current flowing into the network is zero, so it is called "no-flow boundary". Next, the second layer of the matrix neural network is constructed again in this manner and it is considered connecting each other with channels from multiple regions [67]. Izhikevich neural model can be used to represent the dynamical equations of two-layer network, each of which is connected to the nearest neighbor type in a two-dimensional matrix [68]. The collective behaviors of two-layer network can be represented by

$$\begin{cases} \dfrac{dv_{1ij}}{dt} = 0.04v_{1ij}^2 + 5v_{1ij} + 140 - u_{1ij} + I_{1ext} + D_1(v_{1i-1,j} + v_{1i+1,j} + v_{1i,j-1} + v_{1i,j+1} - 4v_{1i,j}), \\ \dfrac{du_{1ij}}{dt} = a(bv_{1ij} - u_{1ij}), \\ \dfrac{dv_{2ij}}{dt} = 0.04v_{2ij}^2 + 5v_{2ij} + 140 - u_{2ij} + I_{2ext} + D_2(v_{2i-1,j} + v_{2i+1,j} + v_{2i,j-1} + v_{2i,j+1} - 4v_{2i,j}) \\ \qquad + k(v_{1ij} - v_{2ij})\delta_{i\alpha}\delta_{j\beta}, \\ \dfrac{du_{2ij}}{dt} = a(bv_{2ij} - u_{2ij}). \end{cases} \tag{3}$$

where subscripts 1 and 2 represent the first and second layer network, and the subscript ($ij$) denotes

the location of the node in the same layer. It can be seen from the structure of the network that each neuron is connected to four neurons, which means that the degree of the network is 4, and the total number of neurons in the network is 40,000, which indicates that the scale of the neural network is defined as 40,000.

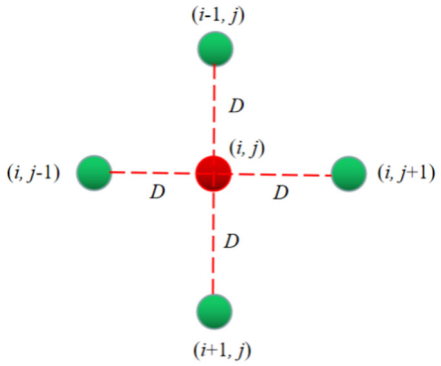


**Figure 1.** Schematic diagram of the connections between neurons. A certain neuron $(i, j)$ is connected to other neurons at four locations, i.e., upper $(i\text{-}1, j)$, lower $(i\text{+}1, j)$, left $(i, j\text{-}1)$ and right $(i, j\text{+}1)$, with connection strength $D$. $D_1$ for first layer (Layer-1) and $D_2$ for second layer (Layer-2).

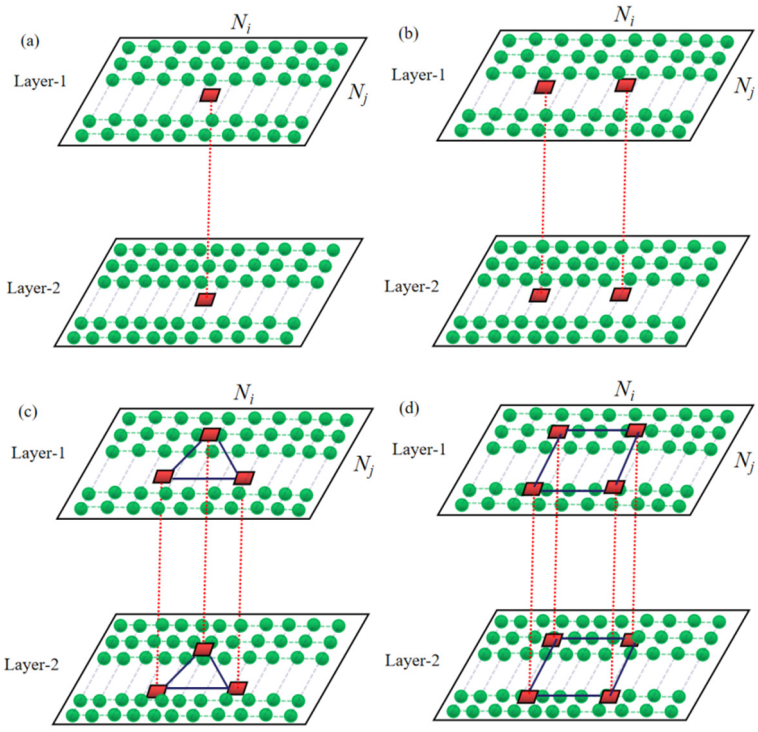


**Figure 2.** Schematic diagram of bi-layer coupled neural network for multi-area channels. The two layers are connected at the nodes (a) $(99 \le \alpha, \beta \le 102)$; (b )$(99 \le \alpha \le 102, 65 \le \beta \le 68)$, $(99 \le \alpha \le 102, 131 \le \beta \le 134)$; (c) $(65 \le \alpha, \beta \le 68)$, $(65 \le \alpha \le 68, 131 \le \beta \le 134)$, $(131 \le \alpha \le 134, 99 \le \beta \le 102)$; (d) $(65 \le \alpha, \beta \le 68)$, $(65 \le \alpha \le 68, 131 \le \beta \le 134)$, $(131 \le \alpha \le 134, 65 \le \beta \le 68)$, $(131 \le \alpha, \beta \le 134)$.

In addition, $D_1$ and $D_2$ in Eq (3) are used to represent the coupling intensity of nearest adjacent nodes in the bi-layer network, and each layer is placed in a two-dimensional matrix, as shown in Figure 2. The intensity of the channel between the two layers is expressed by $k$. $\delta_{i\alpha} = 1$ for $\alpha = i$ and $\delta_{j\beta} = 1$ for $\beta = j$ [69]. Otherwise, $\delta_{i\alpha} = 0$ and $\delta_{j\beta} = 0$. $i$, $j$, $\alpha$ and $\beta$ are integers. For bi-layer neural networks, multiple connection regions are opened at specified locations for generating information exchange between the bi-layer networks, respectively [70]. For example, in Figure 2(a) the connection region is opened between nodes 99 to 102. Figure 2(b) expresses the case that the two layers connect at two local areas ($99 \le \alpha \le 102$, $65 \le \beta \le 68$), ($99 \le \alpha \le 102$, $131 \le \beta \le 134$). For the three local coupling areas ($65 \le \alpha, \beta \le 68$), ($65 \le \alpha \le 68$, $131 \le \beta \le 134$), ($131 \le \alpha \le 134$, $99 \le \beta \le 102$) are investigated in Figure 2(c) and the four local coupling areas ($65 \le \alpha, \beta \le 68$), ($65 \le \alpha \le 68$, $131 \le \beta \le 134$), ($131 \le \alpha \le 134$, $65 \le \beta \le 68$), ($131 \le \alpha, \beta \le 134$) are displayed in Figure 2(d).

### *2.3. Synchronization factor*

To investigate the statistical features of the collective dynamics in the neuronal network more systematically, the synchronization factor R of the neural network is calculated by using the mean-field theory [71]. Synchronization factor R can be calculated as follows

$$\begin{cases} F = \dfrac{1}{N^2}\sum_{j=1}^{N}\sum_{i=1}^{N} v_{ij}; \\ R = \dfrac{\left\langle F^2 \right\rangle - \left\langle F \right\rangle^2}{\dfrac{1}{N^2}\sum_{j=1}^{N}\sum_{i=1}^{N}(\left\langle v_{ij}^2 \right\rangle - \left\langle v_{ij} \right\rangle^2)}. \end{cases} \tag{4}$$

where $v_{ij}$ denotes the membrane potential of each layer nodes $(i, j)$ neuron and it could be calculated from Eq (1). $N$ represents the location of the neuronal node, $N^2$ represents the number of nodes in the network, and symbols < > means that the variables are averaged over time [72]. In particular, if the value of $R$ approaches to 1, it means that the firing behavior of all neurons exhibits a fully synchronized state; when the value of $R$ approaches to 0, it indicates that the neuronal system is in a incompletely synchronized state [73] Previous studies have shown that smaller values of synchronization will support ordered spatial patterns, while larger values of synchronization can develop homogeneous states [74]. Appropriate values of the synchronization factor can generate graceful spatial waves in the network [75].

## 3. Results and discussion

The collective dynamics are calculated by using Euler algorithm with a time step of 0.02 when exploring the spatiotemporal properties of neural networks [76]. In each layer, the 200 × 200 ($N_i$, $N_j$) neuron nodes are uniformly embedded into a two-dimensional square array, with a near-neighbor coupling action between the neurons and considering the no-flow boundary conditions [77]. If there is no special instruction, each neuron in the first layer will be applied an direct current as external force, and the direct current signal applied to each Izhikevich neuron is $I_{ext} = 10$ [78]. On the boundaries of the first layer of the matrix neural network, all random initial values will be generated by random functions as $v_0 = 0.8\xi\ln(i) - 0.2\xi\ln(j) - 3$, $u_0 = -0.8\xi\ln(i) + 0.2\xi\ln(j) - 5$, where $\xi$ represents a random

number between 0 and 1 [79–82]. And initial values of all other neuron will be selected with the same values as ($v_0$, $u_0$) = (0, 0).

### *3.1. Firing patterns and bifurcation analysis of Izhikevich neural model*

The time-series of the neuronal membrane potential are calculated using Euler algorithm method for a certain time period according to the parameters given in Table 1, and the results are plotted in Figure 3. The results in Figure 3(a) illustrate that the membrane potential of Izhikevich neuron in the CH firing mode exhibits a series of cluster firing forms with periodic properties, and each cluster spike exhibits a modal morphology. For the FS firing pattern, as shown in Figure 3(b), the modelling data is derived from inhibitory cortical neurons, where the membrane potential exhibits a periodic firing sequence with an extremely high frequency. The IB discharge pattern is first showing patterned discharge clusters followed by a series of repeated discharge spikes, as shown in Figure 3(c). The neurons in RS states are the most typical neurons in the cortex, and their firing frequency is not too fast because the limitation of their parameters determines that the neurons in RS states have the characteristics of spike frequency adaptation, as shown in Figure 3(d). Unlike neurons in FS states, neurons in RS, CH, and IB states are all used to imitate excitatory neurons, and previous studies have shown that the ratio of excitatory and inhibitory neurons is generally 4:1 in cortical neural network.

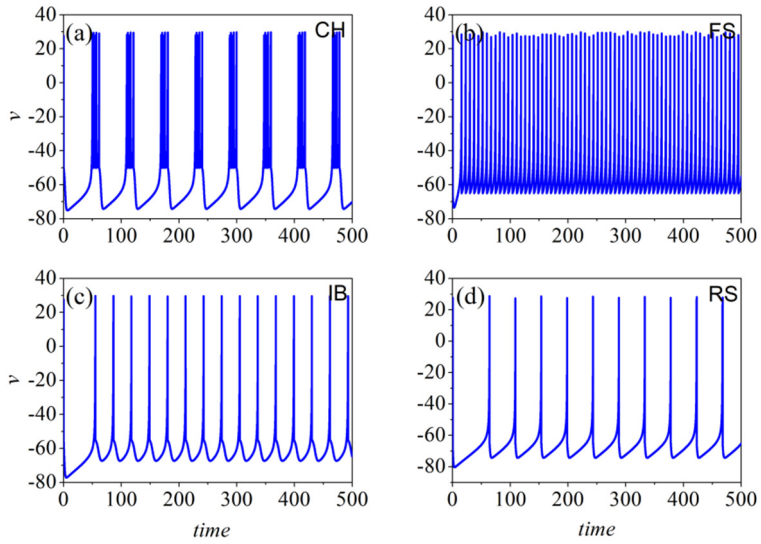


**Figure 3.** Time series of membrane potential of different types of Izhikevich neuronal model.

In order to understand the specific properties of the four different discharge modes of Izhikevich neuron more accurately, the bifurcation of the membrane potential is drawn in Figure 4. It is known that bifurcation often appears in the mathematical research of dynamic systems, which refers to small and continuous changes in system parameters, resulting in sudden changes in the nature of the system. Here, how the change of external stimulation current affect the spike interval of membrane potential is analyzed, and the analysis results obtained are represented by bifurcation of ISI (inter-spike interval). Figure 4(a),(b) make it clear that the peak interval of RS and FS neuronal membrane potential gradually decreases with increasing stimulus current intensity $I$, and the ISI curve shows a tendency to decrease monotonically with the increasing of stimulation current intensity from an overall perspective. These results mean that the RS and FS neurons are in spiking state, and the time interval between discharge

spikes keeps getting smaller. Above conclusions can also be drawn from the time series of membrane potential in Figure 3. However, a obvious difference between the two case is that the peak interval of neuron in FS discharge state is smaller overall than the ISI of neuron in RS discharge state. Figure 4(c),(d) demonstrate that neurons in CH and IB discharge states exhibit more abundant firing properties when the external stimulation current intensity is relatively small. For example, for neuron in CH discharge state, the discharge mode of Izhikevich neuron undergoes the transition from period-2 bursting state to bursting state when the external stimulus current intensity is greater than 3.5. If the external stimulation current intensity is less than 3.5, the discharge mode includes chaotic state, period-3 bursting state and period-2 bursting state. For neuron in IB discharge state, when the external stimulation current intensity increases from 0 to 30, the discharge mode of neurons experiences period-2 bursting state and chaotic discharge, then evolves to period-2 bursting state and finally to spiking state.

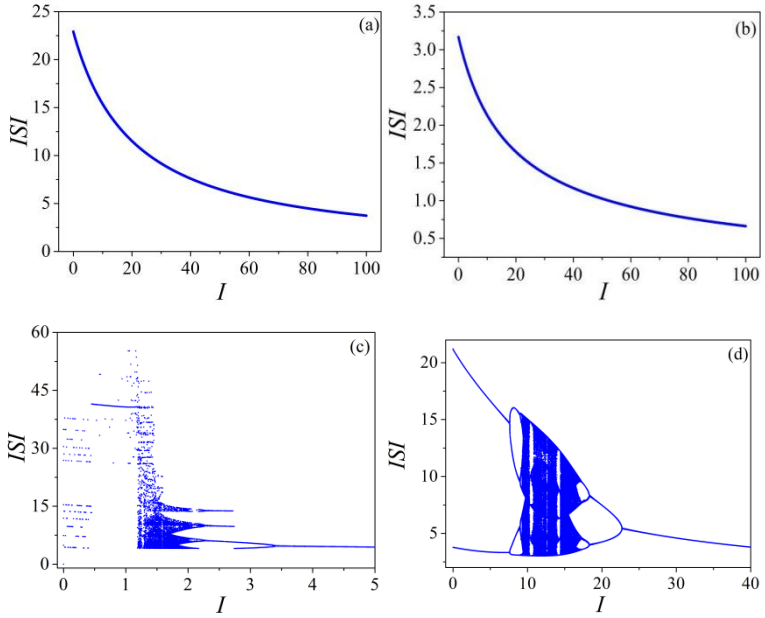


**Figure 4.** Bifurcation diagram of membrane potential changes of four different types of Izhikevich neurons with external stimulation current. (a) RS; (b) FS; (c) CH; (d) IB.

*3.2. Spiral waves and synchronization in Izhikevich neural networks*

In the first layer of the network, the influence of the random boundary value of the matrix network on the spatiotemporal pattern at different times can be observed due to the influence of the external current and the random boundary, as shown in Figure 5. It can be seen that the first layer generates spiral wave induced by random values of boundary under appropriate coupling intensity and external force, and the second layer is in the different states. When the time is relatively small, the advance of traveling wave induced by random boundary can be observed, and some spiral seeds and broken spiral waves gradually appear. As time increases, some single armed and double armed spiral seeds can also be observed.

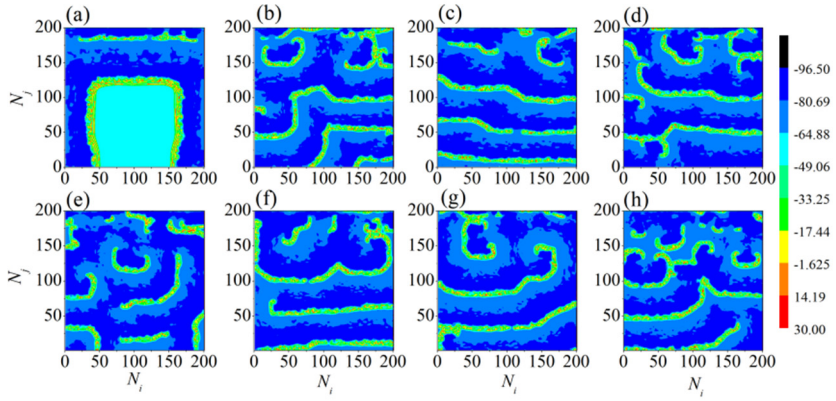


**Figure 5.** The development of spiral wave induced by random values of boundary at different time units under coupling intensity $D_1 = 1.0$ in the first layer network. The snapshots show the spatial distribution for membrane potentials of the neurons in the first layer of coupling intensities $D_1 = 1.0$ over the time. For (a) $t = 100$; (b) $t = 1000$; (c) $t = 2000$; (d) $t = 3000$; (e) $t = 4000$; (f) $t = 5000$; (g) $t = 6000$; (h) $t = 7000$ time units.

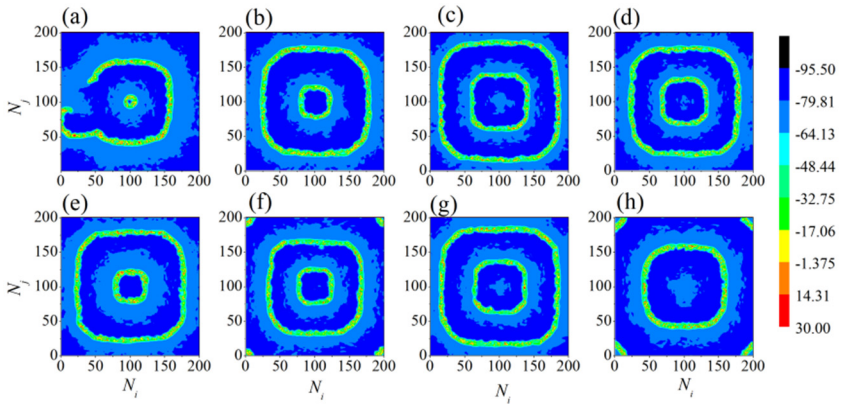


**Figure 6.** The development of spiral wave induced by random values of boundary at different time units under coupling intensity $D_2 = 1.0$ in the second layer network. The snapshots show the spatial distribution for membrane potentials of the neurons in the second layer of coupling intensities $D_1 = 1.0$ and $D_2 = 1.0$ over the time. For (a) $t = 100$; (b) $t = 1000$; (c) $t = 2000$; (d) $t = 3000$; (e) $t = 4000$; (f) $t = 5000$; (g) $t = 6000$; (h) $t = 7000$ time units.

Coupling channels between the two layers are set in multiple areas and spiral wave of first layer affect second layer via the coupling channels. When only one connection channel is set in the middle of the first layer network, the spatiotemporal pattern of the second layer network at different time units are shown in Figure 6. An obvious characteristic of Figure 6 is that all the images at different times in the figure are similar to target waves, except for breakage at 500 time units. Target-like waves tend to move from the boundary to the center of the matrix network, thus different spatiotemporal patterns can be seen at different times. Since the change of the spatiotemporal pattern is not of analytical significance when changing the observation time, we chose to fix the time at 5000 time units and study the impact of changing the neuron coupling strength on the spatiotemporal pattern in the later research.

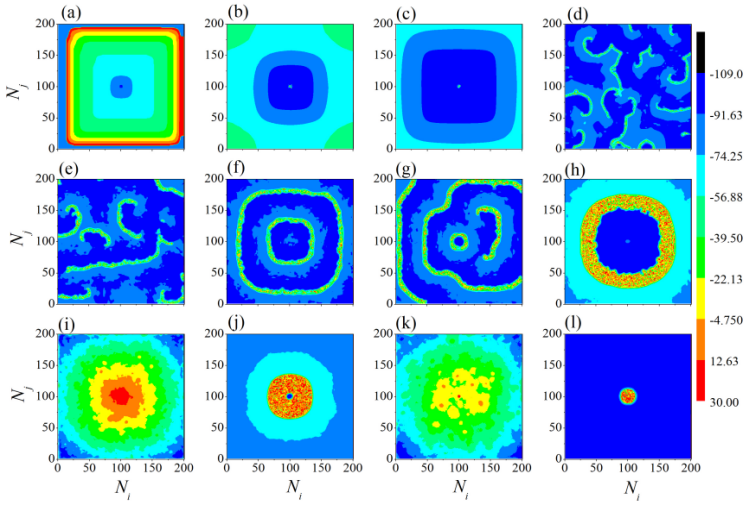


**Figure 7.** The developed pattern of second layer is calculated under different coupling intensity $D_2$ at $t$ = 5000 time units when the two layers connect at one local areas. (a) $D_2$ = 0.1; (b) $D_2$ = 0.2; (c) $D_2$ = 0.3; (d) $D_2$ = 0.4; (e) $D_2$ = 0.7; (f) $D_2$ = 0.9; (g) $D_2$ = 1.1; (h) $D_2$ = 1.4; (i) $D_2$ = 1.6; (j) $D_2$ = 2.3; (k) $D_2$ = 2.9; (l) $D_2$ = 3.0.

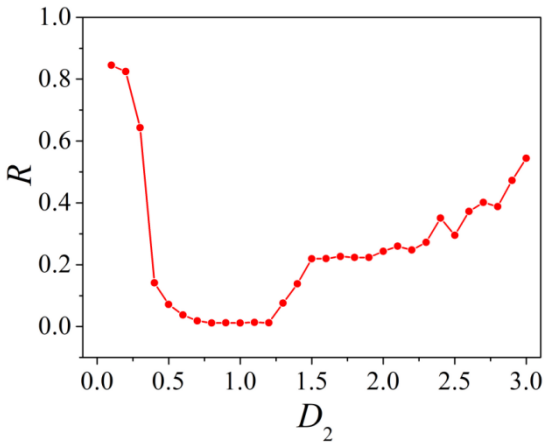


**Figure 8.** Synchronization factor varies with coupling intensity of second layer $D_2$ when the two layers connect at one local areas.

As shown in Figure 7, the developed pattern of second layer is calculated under different coupling intensity $D_2$ at $t$ = 5000 time units when the two layers connect at one local areas. It can be observed that the random boundary value propagates from the boundary of the matrix network to the middle area and after the collision traveling wave it starts to form a spiral seed and a target-like wave in the case of $D_2$ = 0.9. Continue to increase the coupling strength between neurons in the second layer, it can be found that the target-like wave breaks and gradually disappears, and then a target-like wave with high potential is observed in the central area of the network. By further increasing the coupling strength between neurons, it can be observed that the spatiotemporal patterns of the neural network experience the process of convergence → diffusion → re-convergence → re-diffusion. Moreover, when the coupling strength $D_2$ = 3.0, only the neurons in the central area of the neural network are in the discharge state, and the neurons in other areas are inhibited, which may be caused by too large

coupling strength.

According to Eq (4), the synchronization factor is calculated when the coupling strength between neurons in the second layer neural network is changed, and the results are shown in Figure 8. Once you see the image of synchronization factor, you can easily analyze that it is an inverted bell-like shaped curve. In other words, there is an optimal $D_2$ value, which can minimize the synchronization factor $R$. Further analysis shows that when the value of $D_2$ is between 0.4 and 1.3, the synchronization factors are close to the minimum, which means that the synchronization of the neural network is low, but an unexpected phenomenon is that spiral seeds or target-like waves appear in the network. In essence, it can be understood that the synchronization factor is small in this case, and the spatiotemporal patterns of the neural system are orderly arranged, so we can see the above situation. When the coupling strength is small or large, the neural system tends to be stay in homogeneous state, so the synchronization factor is also large. These results are consistent with the previous statement.

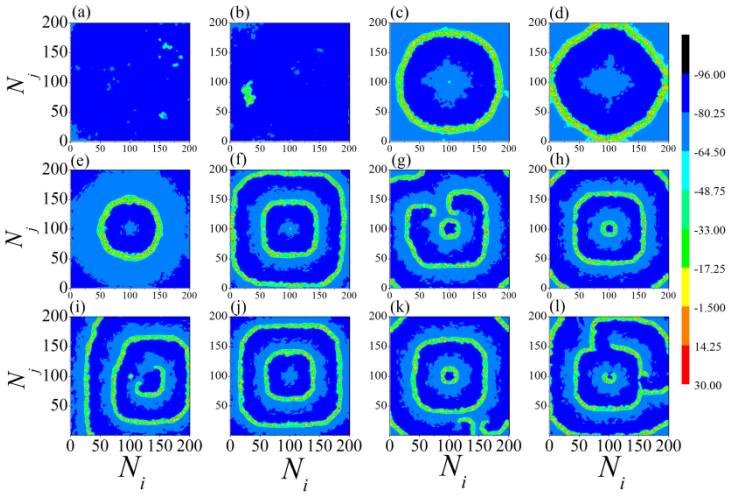


**Figure 9.** The developed pattern of second layer is calculated under different inter-layer connection strength $k$ at $t = 5000$ time units when the two layers connect at one local areas. (a) $k = 0.1$; (b) $k = 0.2$; (c) $k = 0.3$; (d) $k = 0.4$; (e) $k = 0.5$; (f) $k = 0.6$; (g) $k = 0.7$; (h) $k = 1.1$; (i) $k = 1.3$; (j) $k = 1.9$; (k) $k = 2.6$; (l) $k = 3.0$.

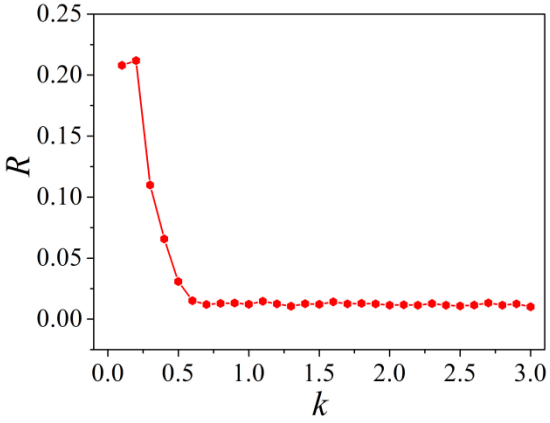


**Figure 10.** Synchronization factor varies with different inter-layer connection strength $k$ when the two layers connect at one local areas.

In the following research, the influence of the inter-layer connection strength on the spatiotemporal patterns in the second layer neural network is studied. As shown in Figure 9, the developed pattern of second layer is calculated under different inter-layer connection strength $k$ at $t$ = 5000 time units when the two layers connect at one local areas. It can be observed that when the inter-layer connection strength is small (for $k$ = 0.1 and $k$ = 0.1), all neurons are basically in a resting state, and only a few neurons oscillate below the threshold. With the increase of inter-layer coupling strength, several relatively complete target-like wave patterns can be observed, and then these ring patterns begin to break, showing a random change rule. This means that the random boundary plays a greater role than the inter-layer coupling strength in the process of generating spiral wave patterns.

The change trend of synchronization factor when changing the inter-layer coupling strength is shown in Figure 10. It is easy to find that the curve is a monotone decreasing function of the inter-layer coupling strength, which indicates that the synchronization of neurons in the neural network will rapidly decrease to a value close to 0 with the increase of the inter-layer coupling strength, and then basically keep fluctuating in a small range. By comparing Figures 9 and 10, it can be found that the spatiotemporal pattern shows that there is neither spiral wave nor spiral seed when the synchronization factor is relatively large. With the further increase of the inter-layer coupling strength, the synchronization factor decreases rapidly, and the target-like wave appears in the spatiotemporal pattern. When the inter-layer coupling strength is further increased and the synchronization factor is reduced to close to 0, the occurred target-like waves begin to break. As mentioned earlier, this is also related to the randomness of random boundary values.

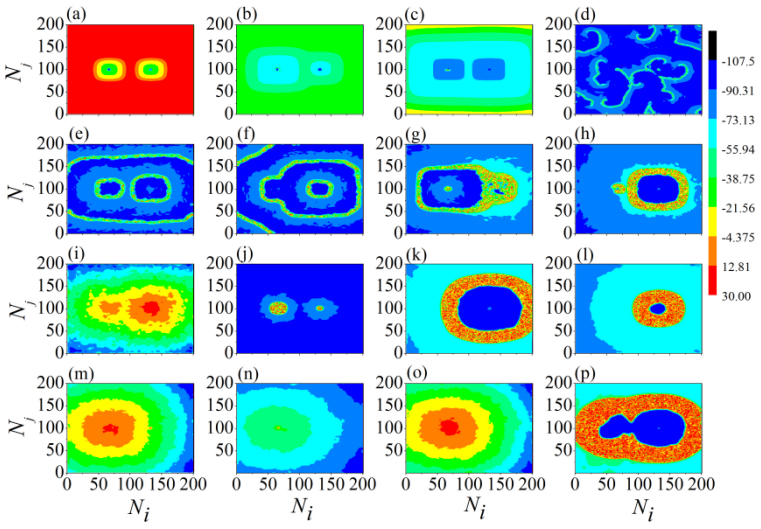


**Figure 11.** The developed pattern of second layer is calculated under different coupling intensity $D_2$ at $t$ = 5000 time units when the two layers connect at two local areas. (a) $D_2$ = 0.1; (b) $D_2$ = 0.2; (c) $D_2$ = 0.3; (d) $D_2$ = 0.4; (e) $D_2$ = 0.9; (f) $D_2$ = 1.1; (g) $D_2$ = 1.2; (h) $D_2$ = 1.4; (i) $D_2$ = 1.5; (j) $D_2$ = 1.8; (k) $D_2$ = 1.9; (l) $D_2$ = 2.1; (m) $D_2$ = 2.2; (n) $D_2$ = 2.3; (o) $D_2$ = 2.5; (p) $D_2$ = 2.6.

In order to understand the impact of the number of connecting channels between layers on the spatiotemporal pattern of the bi-layer neural network, the spatiotemporal pattern in the case of two area connections are studied as well, as shown in Figure 11. From Figure 11(a)–(c), it can be clearly seen that the specific positions of the two connecting regions are obviously different from their

surrounding regions, which indicates that the spiral waves generated by the first layer of network have a great impact on the spatiotemporal pattern of the second layer. When the connection strength $D_2$ between neurons in the second layer increases to 0.4, obvious spiral seeds can be observed, including single arm and double arm. If we continue to increase the connection strength between neurons, it is found that the spatiotemporal pattern starts to change into the form of target-like waves, but the appearance of complete target-like waves can hardly be observed. Another obvious feature is that the area where the two connecting channels are located has a great impact on the neural network of the second layer, and no matter what the coupling strength is, this impact basically exists.

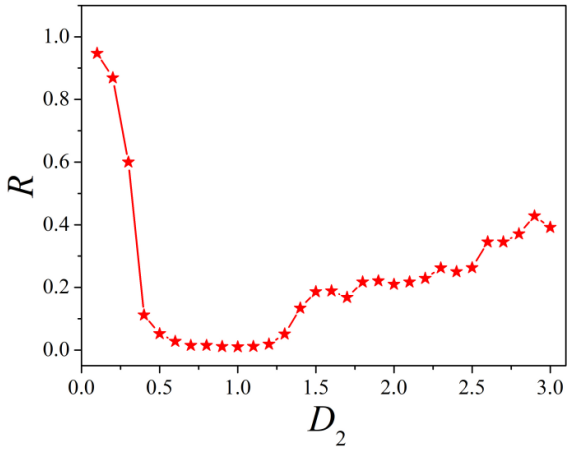


**Figure 12.** Synchronization factor varies with coupling intensity of second layer $D_2$ when the two layers connect at two local areas.

When the two layers are connected at two local areas, the synchronization factor changing with the coupling intensity of the second layer is shown in Figure 12, and the curve in the form of anti-resonance is observed again in this image. It can be found that when the variation range of $D_2$ is from 0.5 to 1.2, the value of synchronization factor $R$ is the relative minimum, however the synchronization factor is relatively large when the coupling strength is small. This anti-resonance curve shows that there is a certain range of coupling strength that can inhibit the synchronization of neurons in the neural network.

Considering that the inter-layer connection strength also affects the spatiotemporal dynamics of the second layer neural network, the developed pattern of second layer under different inter-layer connection strength is shown in Figure 13. At the same time, if you compare Figures 13 and 14, one can find the same rule as described above, that is, the synchronization factor is relatively large when the inter-layer coupling strength is small, and no spiral seeds or spiral waves are displayed in the network. If the inter-layer coupling strength $k$ is selected as 0.2, the synchronization factor shows a maximum value that is not very obvious, showing the form of "resonance". If the inter-layer connection strength is continued to increase, it will again get the result that the synchronization factor decreases rapidly and remains near zero. However, no matter whether the value of synchronization factor is 0 or not, broken spiral seeds and incomplete target like waves can be observed in the spatiotemporal model. Among these broken spiral seeds, the traces of the connection channels in the two areas can also be clearly seen, indicating that the location of the connection channels really plays a crucial role in the spatiotemporal pattern in the second layer network.

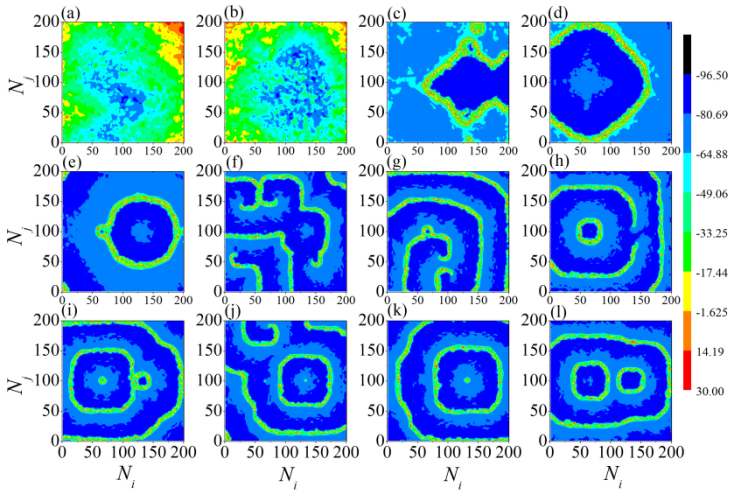


**Figure 13.** The developed pattern of second layer is calculated under different inter-layer connection strength $k$ at $t = 5000$ time units when the two layers connect at two local areas. (a) $k = 0.1$; (b) $k = 0.2$; (c) $k = 0.3$; (d) $k = 0.4$; (e) $k = 0.5$; (f) $k = 0.6$; (g) $k = 0.7$; (h) $k = 0.9$; (i) $k = 1.1$; (j) $k = 1.4$; (k) $k = 2.0$; (l) $k = 2.4$.

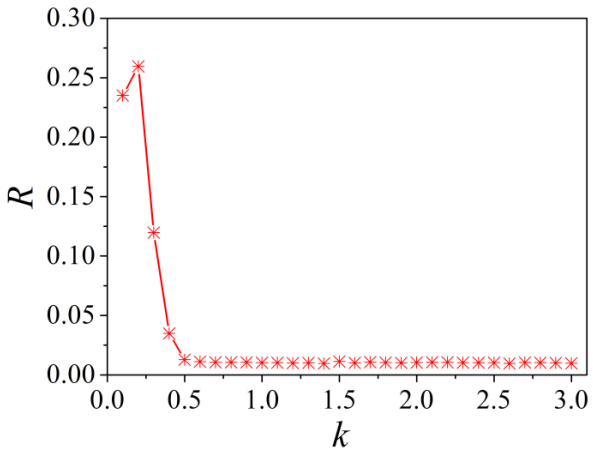


**Figure 14.** Synchronization factor varies with different inter-layer connection strength $k$ when the two layers connect at two local areas.

In the following research, the bisection and trisection points of the spatial location in the second layer matrix networks are found out and they are determines as three connection areas to connect the two layers respectively. The developed pattern of second layer is calculated under different coupling intensity $D_2$ at $t = 5000$ time units when the two layers connect at three local areas, which is plotted in Figure 15. It can be observed that the three connection regions have a great impact on the spatiotemporal pattern of the second layer neural network. The diversity of the spatiotemporal pattern is derived from the changes in the signals of the three connection channels. When the signals come from the three channels collide and interact, rich and varied spatiotemporal pattern can be generated in the entire network. With the generation of the collision and the further propagation of the signal, the broken spiral wave and double armed spiral seed appear. If the coupling strength between neurons is further increased, the appearance of target-like waves can also be observed, and a large number of neurons may appear in some certain regular area and discharge intensively at the same time.

Synchronization factor varies with coupling intensity of second layer $D_2$ is plotted in Figure 16 when the two layers connect at three local areas. As in the previous $R$-$D_2$ curves, the relationship between synchronization factor and coupling strength between neurons in the second layer presents the form of "anti-resonance", indicating that there is a certain range of coupling strength which can make the synchronization of neural network the lowest. When the connection channel becomes four regions, the same conclusion can be obtained, as shown in Figure 20. In general, the synchronization factor changes with $D_2$ in the form of anti-resonance when the coupling strength between neurons in the second layer is changed. This conclusion is valid regardless of how many connection channels exist between the two layers of networks.

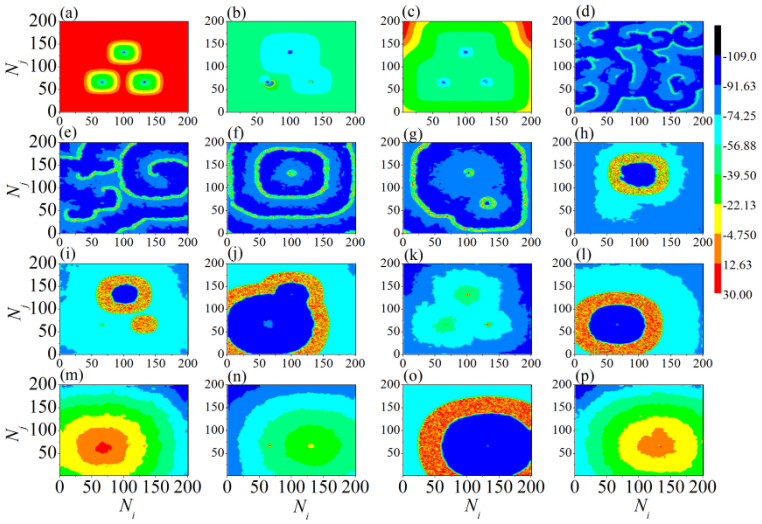


**Figure 15.** The developed pattern of second layer is calculated under different coupling intensity $D_2$ at $t$ = 5000 time units when the two layers connect at three local areas. (a) $D_2$ = 0.1; (b) $D_2$ = 0.2; (c) $D_2$ = 0.3; (d) $D_2$ = 0.4; (e) $D_2$ = 0.8; (f) $D_2$ = 0.9; (g) $D_2$ = 1.0; (h) $D_2$ = 1.4; (i) $D_2$ = 1.7; (j) $D_2$ = 1.8; (k) $D_2$ = 1.9; (l) $D_2$ = 2.1; (m) $D_2$ = 2.4; (n) $D_2$ = 2.6; (o) $D_2$ = 2.9; (p) $D_2$ = 3.0.

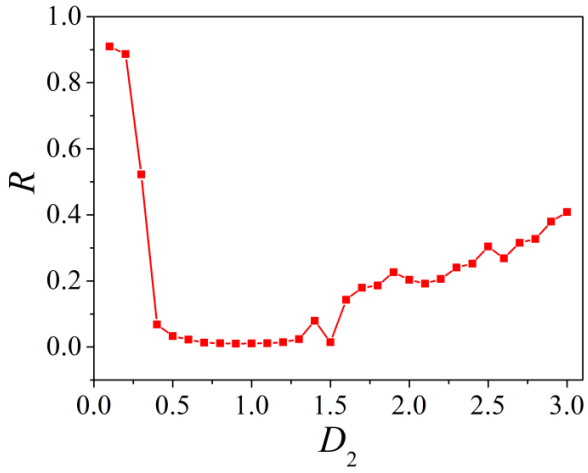


**Figure 16.** Synchronization factor varies with coupling intensity of second layer $D_2$ when the two layers connect at three local areas.

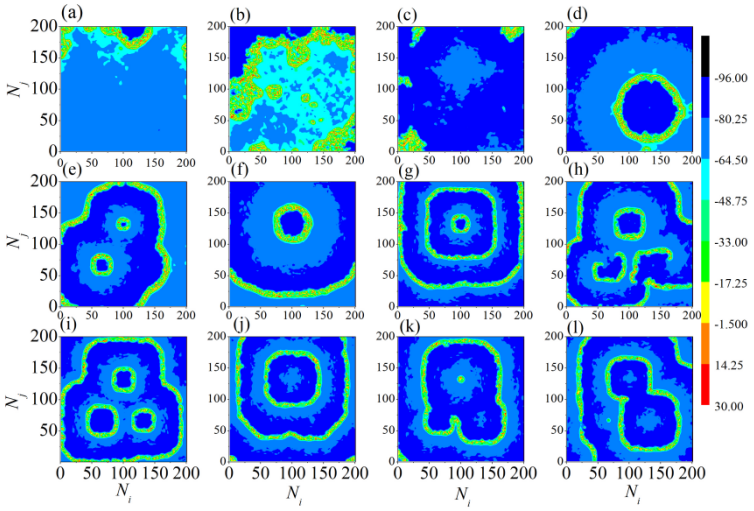


**Figure 17.** The developed pattern of first layer is calculated under different inter-layer connection strength $k$ at $t$ = 5000 time units when the two layers connect at three local areas. (a) $k = 0.1$; (b) $k = 0.2$; (c) $k = 0.3$; (d) $k = 0.4$; (e) $k = 0.5$; (f) $k = 0.6$; (g) $k = 0.7$; (h) $k = 0.8$; (i) $k = 1.1$; (j) $k = 1.4$; (k) $k = 1.8$; (l) $k = 3.0$.

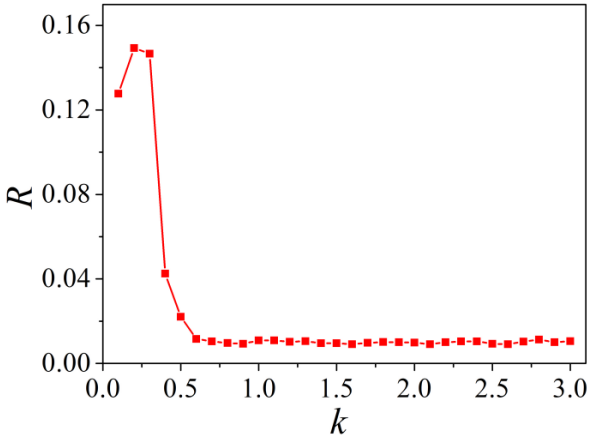


**Figure 18.** Synchronization factor varies with different inter-layer connection strength $k$ when the two layers connect at three local areas.

If the inter-layer connection strength is changed, whether the connection channels between the two layers of neural networks are selected as 3 or 4, the overall change trend of the spatiotemporal pattern is basically consistent, as shown in Figures 17 and 21. No matter how many connection areas are between the two layers, one can clearly observe the effect of the connection channel on the second layer network in the spatiotemporal pattern. In the above two cases, the synchronization factor changing with inter-layer connection strength are plotted in Figures 18 and 22. Although these two figures are basically consistent with the previous *R*-*k* curve on the whole, they show resonance peaks similar to resonance when the inter-layer coupling strength is small. Under other inter-layer coupling strengths, there is still a random transition from the broken spiral seed to the target-like wave.

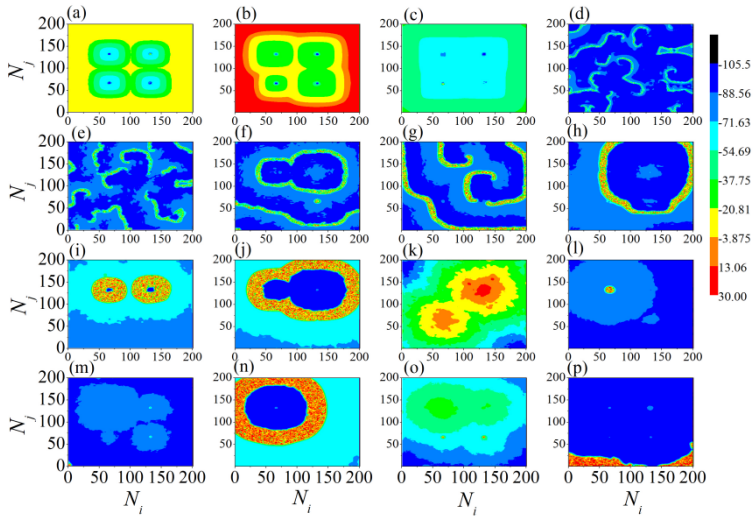


**Figure 19.** The developed pattern of second layer is calculated under different coupling intensity $D_2$ at $t$ = 5000 time units when the two layers connect at four local areas. (a) $D_2$ = 0.1; (b) $D_2$ = 0.2; (c) $D_2$ = 0.3; (d) $D_2$ = 0.4; (e) $D_2$ = 0.7; (f) $D_2$ = 0.9; (g) $D_2$ = 1.3; (h) $D_2$ = 1.4; (i) $D_2$ = 1.5; (j) $D_2$ = 1.6; (k) $D_2$ = 1.7; (l) $D_2$ = 1.8; (m) $D_2$ = 2.0; (n) $D_2$ = 2.1; (o) $D_2$ = 2.4; (p) $D_2$ = 3.0.

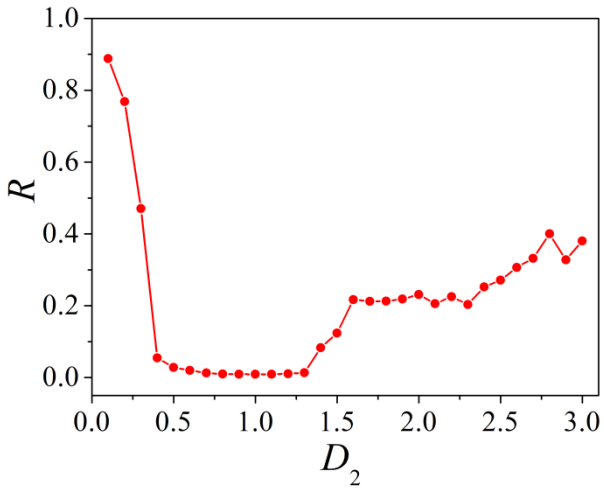


**Figure 20.** Synchronization factor varies with coupling intensity of second layer $D_2$ when the two layers connect at four local areas.

Figure 19 shows the spatiotemporal pattern when there are four connection regions between the two layers of networks. It can be seen that when the coupling strength of neurons in the second layer is 0.1, the spatiotemporal pattern in the network presents a basically symmetrical pattern. Then, this symmetry is destroyed with the increase of coupling strength between neurons. The reason may be that the increase of coupling strength also leads to the increase of randomness, which leads to the loss of symmetry. In the subsequent images, spiral seeds and broken target-like waves can still be observed. The analysis of these images tells us that when the coupling strength between neurons in the second layer is changed, the spatiotemporal patterns in the second layer of neural network may appear in a variety of forms, and the corresponding synchronization factor may appear in the form of anti-

resonance with the change of coupling strength. On the other hand, a curve that is a monotone decreasing function as a whole can be observed when the coupling strength between layers is changed. Figures 20–22 have been discussed previously and will not be repeated here.

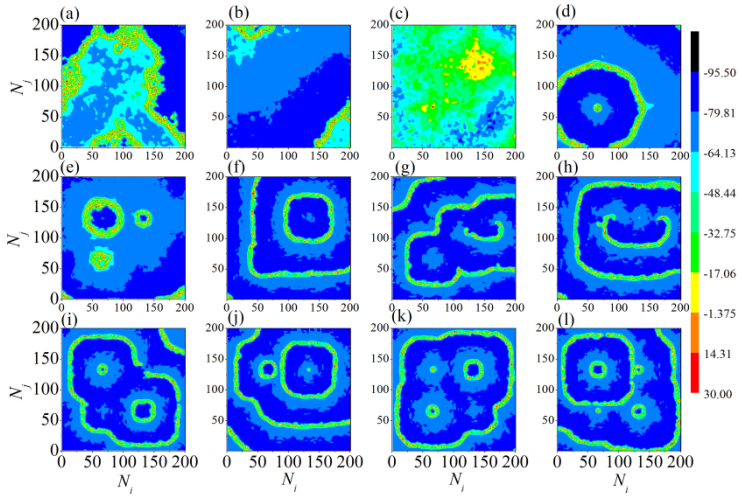


**Figure 21.** The developed pattern of first layer is calculated under different coupling intensity $D_2$ at $t$ = 5000 time units when the two layers connect at four local areas. (a) $k$ = 0.1; (b) $k$ = 0.2; (c) $k$ = 0.3; (d) $k$ = 0.4; (e) $k$ = 0.5; (f) $k$ = 0.6; (g) $k$ = 0.8; (h) $k$ = 1.4; (i) $k$ = 1.5; (j) $k$ = 1.8; (k) $k$ = 2.6; (l) $k$ = 3.0.

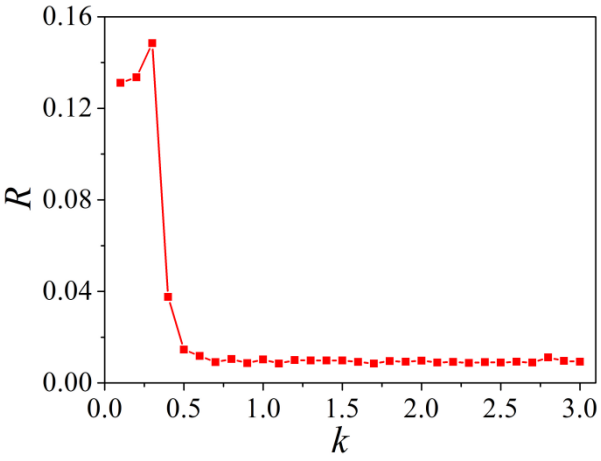


**Figure 22.** Synchronization factor varies with different inter-layer connection strength $k$ when the two layers connect at four local areas.

## 4. Conclusions

Based on four kinds of firing patterns of Izhikevich neuronal model, a bi-layer neural network with multi-channel connection is constructed using numerical simulation. Each layer of network is composed of 200 × 200 Izhikevich neurons to model a two-dimensional matrix network, and random functions are applied at the boundary of first layer of network. The spiral wave in the first layer is

transmitted to the second layer through multiple channels, and the spatiotemporal mode and network synchronization in the second layer are studied. By means of simulation, four different firing modes of neurons are discussed respectively, and the bifurcation of the membrane potential are studied. Then the formation and breaking mechanism of spiral wave in the two-layer network are studied as the coupling strength between neurons in the second layer and the inter-layer connection strength increase. With the development of the research, the synchronization properties of neural networks are explored by changing the coupling strength between neurons in the second layer as well as the inter-layer connection strength.

Obtained results indicate that only when the firing mode of the Izhikevich neuron constituting the matrix neural network is in RS state, the emergence and disappearance of spiral waves can be observed in the network, while the formation of spiral wave seeds cannot be observed in the network if it is composed of other firing modes such as FS, IB and CH. Further research shows that the variation of synchronization factor with coupling strength between adjacent neurons in the second layer shows an inverse bell-like curve in the form of "inverse resonance", but the variation of synchronization factor with inter-layer connection strength is a curve which is approximately monotonically decreasing. No matter how many connection areas are between the two layers of neural networks, spiral waves can be observed in the second layer of matrix neural networks, even the appearance of target-like waves can be observed under some certain conditions. Furthermore, we find that the more important phenomenon is that lower synchronicity is helpful to develop spatiotemporal patterns.

The study of the coupling strength and the influence of random boundaries in the neural networks constructed by Izhikevich neurons on the spatiotemporal behavior can be instructive to further explore the signal propagation in the cerebral cortical neural networks.

## Acknowledgments

This work is supported by Science and Technology Project of Jiangxi Provincial Department of Education under Grants No. GJJ203111, Science and Technology Project of Yuzhang Normal University under Grants No. YZYB-21-17, and Talent Introduction Project (No. NGRCZX-22-07), Special Fund for Doctor of Science and Technology Program of Nanchang Institute of Science and Technology under Grants No. NGKJ-21-03.

## Conflict of interest

The authors declare there is no conflict of interest.

## Author statement

Guowei Wang: Conceptualization, Methodology, Software, Visualization, Investigation, Writing-Reviewing and Editing; Yan Fu: Data curation, Writing-Original draft preparation, Supervision, Software, Validation.

## Data availability statement

The authors confirm that the data supporting the findings of this study are available within the article.

## References


1. V. S. Zykov, Spiral wave initiation in excitable media, *Philos. Trans. R. Soc. A*, **376** (2018), 20170379. https://doi.org/10.1098/rsta.2017.0379
2. F. Amdjadi, A numerical method for the dynamics and stability of spiral waves, *Appl. Math. Comput.*, **217** (2010), 3385–3391. https://doi.org/10.1016/j.amc.2010.09.002
3. A. Bukh, G. Strelkova, V. Anishchenko, Spiral wave patterns in a two-dimensional lattice of nonlocally coupled maps modeling neural activity, *Chaos Solitons Fractals*, **120** (2019), 75–82. https://doi.org/10.1016/j.chaos.2018.11.037
4. A. V. Bukh, E. Schöll, V. S. Anishchenko, Synchronization of spiral wave patterns in two-layer 2D lattices of nonlocally coupled discrete oscillators, *Chaos*, **29** (2019), 053105. https://doi.org/10.1063/1.5092352
5. A. V. Bukh, V. S. Anishchenko, Spiral, target, and chimera wave structures in a two- dimensional ensemble of nonlocally coupled van der Pol oscillators, *Tech. Phys. Lett.*, **45** (2019), 675–678. https://doi.org/10.1134/S1063785019070046
6. E. M. Cherry, F. H. Fenton, Visualization of spiral and scroll waves in simulated and experimental cardiac tissue, *New J. Phys.*, **10** (2008), 125016. https://doi.org/10.1088/1367-2630/10/12/125016
7. X. Cui, X. Huang, Z. Di, Target wave imagery in nonlinear oscillatory systems, *Europhys. Lett.*, **112** (2015), 54003. https://doi.org/10.1209/0295-5075/112/54003
8. B. W. Li, X. Gao, Z. G. Deng, H. P. Ying, H. Zhang, Circular-interface selected wave patterns in the complex Ginzburg-Landau equation, *Europhys. Lett.*, **91** (2010), 34001. https://doi.org/10.1209/0295-5075/91/34001
9. R. Wang, J. Li, M. Du, J. Lei, Y. Wu, Transition of spatiotemporal patterns in neuronal networks with chemical synapses, *Commun. Nonlinear Sci. Numer. Simul.*, **40** (2016), 80–88. https://doi.org/10.1016/j.cnsns.2016.04.018
10. M. Y. Ge, G. W. Wang, Y. Jia, Influence of the Gaussian colored noise and electromagnetic radiation on the propagation of subthreshold signals in feedforward neural networks, *Sci. China Technol. Sci.*, **64** (2021), 847–857. https://doi.org/10.1007/s11431-020-1696-8
11. A. V. Bukh, V. S. Anishchenko, Features of the synchronization of spiral wave structures in interacting lattices of nonlocally coupled maps, *Russ. J. Nonlinear Dyn.*, **16** (2020), 243–257. https://doi.org/10.20537/nd200202
12. M. C. Cai, J. T. Pan, H. Zhang, Electric-field-sustained spiral waves in subexcitable media, *Phys. Rev. E*, **86** (2012), 016208. https://doi.org/10.1103/PhysRevE.86.016208
13. J. X. Chen, J. R. Xu, H. P. Ying, Resonant drift of spiral waves induced by mechanical deformation, *Int. J. Mod. Phys. B*, **2** **4**(2012), 5733–5741. https://doi.org/10.1142/S0217979210056323
14. J. Chen, L. Peng, Y. Zhao, S. You, N. Wu, H. Ying, et al., Dynamics of spiral waves driven by a rotating electric field, *Commun. Nonlinear Sci. Numer. Simul.*, **19** (2014), 60–66. https://doi.org/10.1016/j.cnsns.2013.03.010
15. C. N. Wang, J. Ma, B. Hu, W. Jin, Formation of multi-armed spiral waves in neuronal network induced by adjusting ion channel conductance, *Int. J. Mod. Phys. B*, **29** (2015), 1550043. https://doi.org/10.1142/S0217979215500435

16. J. Gao, Q. Wang, H. Lv, Super-spiral structures of bi-stable spiral waves and a new instability of spiral waves, *Chem. Phys. Lett.*, **685** (2017), 205–209. https://doi.org/10.1016/j.cplett.2017.07.061
17. J. Z. Gao, S. X. Yang, L. L. Xie, J. H. Gao, Synchronizing spiral waves in a coupled Rössler system, *Chin. Phys. B*, **20** (2011), 030505. https://doi.org/10.1088/1674-1056/20/3/030505
18. Y. Nishitani, C. Hosokawa, Y. Mizuno-Matsumoto, T. Miyoshi, S. Tamura, Classification of spike wave propagations in a cultured neuronal network: Investigating a brain communication mechanism, *AIMS Neurosci.*, **4** (2017), 1–13. https://doi.org/10.3934/Neuroscience.2017.1.1
19. J. Ma, Y. Xu, J. Tang, C. Wang, Defects formation and wave emitting from defects in excitable media, *Commun. Nonlinear Sci. Numer. Simul.*, **34** (2016), 55–65. https://doi.org/10.1016/j.cnsns.2015.10.013
20. R. Sirovich, L. Sacerdote, A. E. P. Villa, Cooperative behavior in a jump diffusion model for a simple network of spiking neurons, *Math. Biosci. Eng.*, **11** (2014), 385–401. https://doi.org/10.3934/mbe.2014.11.385
21. A. Gholami, O. Steinbock, V. Zykov, E. Bodenschatz, Flow-driven instabilities during pattern formation of Dictyostelium discoideum, *New J. Phys.*, **17** (2015), 063007. https://doi.org/10.1088/1367-2630/17/6/063007
22. S. Gong, X. Tang, J. Zheng, M. A. Nascimento, H. Varela, Y. Zhao, et al., Amplitude-modulated spiral waves arising from a secondary Hopf bifurcation in mixed-mode oscillatory media, *Chem. Phys. Lett.*, **567** (2013), 55–59. https://doi.org/10.1016/j.cplett.2013.02.042
23. S. Blankenburg, B. Lindner, The effect of positive interspike interval correlations on neuronal information transmission, *Math. Biosci. Eng.*, **13** (2016), 461–481. https://doi.org/10.3934/mbe.2016001
24. E. Griv, I. G. Jiang, D. Russeil, Parameters of the galactic density-wave spiral structure, line-of-sight velocities of 156 star-forming regions, *New Astronomy*, **35** (2015), 40–47. https://doi.org/10.1016/j.newast.2014.09.001
25. H. G. Gu, B. Jia, Y. Y. Li, G. R. Chen, White noise-induced spiral waves and multiple spatial coherence resonances in a neuronal network with type I excitability, *Phys. A*, **392** (2013), 1361–1374. https://doi.org/10.1016/j.physa.2012.11.049
26. S. Guo, Q. Dai, H. Cheng, H. Li, F. Xie, J. Yang, Spiral wave chimera in two-dimensional nonlocally coupled Fitzhugh-Nagumo systems, *Chaos Solitons Fractals*, **114** (2018), 394–399. https://doi.org/10.1016/j.chaos.2018.07.029
27. J. Ma, J. Tang, C. N. Wang, Y. Jia, Propagation and synchronization of $Ca^{2+}$ spiral waves in excitable media, *Int. J. Bifurcation Chaos*, **21** (2011), 587–601. https://doi.org/10.1142/S0218127411028635
28. C. Hall, D. Forgan, K. Rice, T. J. Harries, P. D. Klaassen, B. Biller, Directly observing continuum emission from self-gravitating spiral waves, *Mon. Not. R. Astron. Soc.*, **458** (2016), 306–318. https://doi.org/10.1093/mnras/stw296
29. L. H. Zhao, S. Wen, M. Xu, K. Shi, S. Zhu, T. Huang, PID control for output synchronization of multiple output coupled complex networks, *IEEE Trans. Network Sci. Eng.*, **9** (2022), 1553–1566. https://doi.org/10.1109/TNSE.2022.3147786
30. L. H. Zhao, S. Wen, C. Li, K. Shi, T. Huang, A recent survey on control for synchronization and passivity of complex networks, *IEEE Trans. Network Sci. Eng.*, **9** (2022), 4235–4254. https://doi.org/10.1109/TNSE.2022.3196786

31. G. Hu, X. Li, S. Lu, Y. Wang, Bifurcation analysis and spatiotemporal patterns in a diffusive predator-prey model, *Int. J. Bifurcation Chaos*, **24** (2014), 1450081. https://doi.org/10.1142/S0218127414500813
32. H. Hu, X. Li, Fang, X. Fu, L. Ji, Q. Li, Inducing and modulating spiral waves by delayed feedback in a uniform oscillatory reaction-diffusion system, *Chem. Phys.*, **371** (2010), 60–65. https://doi.org/10.1016/j.chemphys.2010.04.004
33. M. Montesinos, S. Perez, S. Casassus, S. Marino, J. Cuadra, V. Christiaens, Spiral waves triggered by shadows in transition disks, *Astrophys. J. Lett.*, **823** (2016), L8. https://doi.org/10.3847/2041-8205/823/1/L8
34. C. Huang, X. Cui, Z. Di, Competition of spiral waves in heterogeneous CGLE systems, *Nonlinear Dyn.*, **98** (2019), 561–571. https://doi.org/10.1007/s11071-019-05212-1
35. X. Huang, W. Xu, J. Liang, K. Takagaki, X. Gao, J. Wu, Spiral wave dynamics in neocortex, *Neuron*, **68** (2010), 978–990. https://doi.org/10.1016/j.neuron.2010.11.007
36. I. A. Shepelev, S. S. Muni, T. E. Vadivasova, Synchronization of wave structures in a heterogeneous multiplex network of 2D lattices with attractive and repulsive intra-layer coupling, *Chaos*, **31** (2021), 021104. https://doi.org/10.1063/5.0044327
37. S. Jacquir, S. Binczak, B. Xu, G. Laurent, D. Vandroux, P. Athias, et al., Investigation of micro spiral waves at cellular level using a microelectrode arrays technology, *Int. J. Bifurcation Chaos*, **21** (2011), 209–223. https://doi.org/10.1142/S0218127411028374
38. D. Jaiswal, J. C. Kalita, Novel high-order compact approach for dynamics of spiral waves in excitable media, *Appl. Math. Modell.*, **77** (2020), 341–359. https://doi.org/10.1016/j.apm.2019.07.029
39. A. R. Nayak, R. Pandit, Spiral-wave dynamics in ionically realistic mathematical models for human ventricular tissue: the effects of periodic deformation, *Front. Physiol.*, **5** (2014), 207–225. https://doi.org/10.3389/fphys.2014.00207
40. V. N. Kachalov, N. N. Kudryashova, K. I. Agladze, Spontaneous spiral wave breakup caused by pinning to the tissue defect, *JETP Lett.*, **104** (2016), 635–638. https://doi.org/10.1134/S0021364016210025
41. N. V. Kandaurova, V. S. Chekanov, V. V. Chekanov, Observation of the autowave process in the near-electrode layer of the magnetic fluid, Spiral waves formation mechanism, *J. Mol. Liq.*, **272** (2018), 828–833. https://doi.org/10.1016/j.molliq.2018.10.073
42. C. Gu, P. Wang, T. Weng, H. Yang, J. Rohling Heterogeneity of neuronal properties determines the collective behavior of the neurons in the suprachiasmatic nucleus, *Math. Biosci. Eng.*, **16** (2019), 1893–1913. https://doi.org/10.3934/mbe.2019092
43. F. M. G. Magpantay, X. Zou, Wave fronts in neuronal fields with nonlocal post-synaptic axonal connections and delayed nonlocal feedback connections, *Math. Biosci. Eng.*, **7** (2010), 421–442. https://doi.org/10.3934/mbe.2010.7.421
44. S. Kawaguchi, Propagating wave segment under global feedback, *Eur. Phys. J. B.*, **87** (2014), 1–10. https://doi.org/10.1140/epjb/e2014-40999-1
45. T. Y. Li, G. W. Wang, D. Yu, Q. Ding, Y. Jia, Synchronization mode transitions induced by chaos in modified Morris-Lecar neural systems with weak coupling, *Nonlinear Dyn.*, **108** (2022), 2611–2625. https://doi.org/10.1007/s11071-022-07318-5

46. M. Mehrabbeik, F. Parastesh, J. Ramadoss, K. Rajagopal, H. Namazi, S. Jafari, Synchronization and chimera states in the network of electrochemically coupled memristive Rulkov neuron maps, *Math. Biosci. Eng.*, **18** (2021), 9394–9409. https://doi.org/10.3934/mbe.2021462
47. N. E. Kouvaris, S. Hata, A. D. Guilera, Pattern formation in multiplex networks, *Sci. Rep.* **5** (2015), 1–9. https://doi.org/10.1038/srep10840
48. P. Kuklik, P. Sanders, L. Szumowski, J. J. Żebrowski, Attraction and repulsion of spiral waves by inhomogeneity of conduction anisotropy—a model of spiral wave interaction with electrical remodeling of heart tissue, *J. Biol. Phys.*, **39** (2013), 67–80. https://doi.org/10.1007/s10867-012-9286-4
49. P. Kuklik, L. Szumowski, P. Sanders, J. J. Żebrowski, Spiral wave breakup in excitable media with an inhomogeneity of conduction anisotropy, *Comput. Biol. Med.*, **40** (99), 775–780. https://doi.org/10.1016/j.compbiomed.2010.07.005
50. P. Kuklik, C. X. Wong, A. G. Brooks, J. J. Żebrowski, Prashanthan Sanders, Role of spiral wave pinning in inhomogeneous active media in the termination of atrial fibrillation by electrical cardioversion, *Comput. Biol. Med.*, **40** (2010), 363–372. https://doi.org/10.1016/j.compbiomed.2010.02.001
51. S. Kumar, A. Das, Spiral waves in driven strongly coupled Yukawa systems, *Phys. Rev. E*, **97** (2018), 063202. https://doi.org/10.1103/PhysRevE.97.063202
52. O. Kwon, T. Y. Kim, K. J. Lee, Period-2 spiral waves supported by nonmonotonic wave dispersion, *Phys. Rev. E*, **82** (2010), 046213. https://doi.org/10.1103/PhysRevE.82.046213
53. D. Lacitignola, B. Bozzini, I. Sgura, Spatio-temporal organization in a morphochemical electrodeposition model: Analysis and numerical simulation of spiral waves, *Acta Appl. Math.*, **132** (2014), 377–389. https://doi.org/10.1007/s10440-014-9910-3
54. D. Lacitignola, I. Sgura, B. Bozzini, T. Dobrovolska, I. Krastev, Spiral waves on the sphere for an alloy electrodeposition model, *Commun. Nonlinear Sci. Numer. Simul.*, **79** (2019), 104930. https://doi.org/10.1016/j.cnsns.2019.104930
55. B. W. Li, H. Dierckx, Spiral wave chimeras in locally coupled oscillator systems, *Phys. Rev. E*, **93** (2016), 020202. https://doi.org/10.1103/PhysRevE.93.020202
56. F. Li, J. Ma, Selection of spiral wave in the coupled network under Gaussian colored noise, *Int. J. Mod. Phys. B*, **27** (2013), 1350115. https://doi.org/10.1142/S0217979213501154
57. G. Z. Li, Y. Q. Chen, G. N. Tang, J. X. Liu, Spiral wave dynamics in a response system subjected to a spiral wave forcing, *Chin. Phys. Lett.*, **28** (2011), 020504. https://doi.org/10.1088/0256-307X/28/2/020504
58. J. Ma, Q. Liu, H. Ying, Y. Wu, Emergence of spiral wave induced by defects block, *Commun. Nonlinear Sci. Numer. Simul.*, **18** (2013), 1665–1675. https://doi.org/10.1016/j.cnsns.2012.11.016
59. T. C. Li, X. Gao, F. F. Zheng, D. B. Pan, B. Zheng, H. Zhang, A theory for spiral wave drift induced by ac and polarized electric fields in chemical excitable media, *Sci. Rep.*, **7** (2017), 1–9. https://doi.org/10.1038/s41598-016-0028-x
60. T. C. Li, B. W. Li, B. Zheng, H. Zhang, A. Panfilov, H. Dierckx, A quantitative theory for phase-locking of meandering spiral waves in a rotating external field, *New J. Phys.*, **21** (2019), 043012. https://doi.org/10.1088/1367-2630/ab096a
61. J. Ma, J. Tang, A. H. Zhang, Y. Jia, Robustness and breakup of the spiral wave in a two-dimensional lattice network of neurons, *Sci. China: Phys. Mech. Astron.*, **53** (2010), 672–679. https://doi.org/10.1007/s11430-010-0050-y

62. S. B. Liu, Y. Wu, J. J. Li, Y. Xie, N. Tan, The dynamic behavior of spiral waves in stochastic Hodgkin-Huxley neuronal networks with ion channel blocks, *Nonlinear Dyn.*, **73** (2013), 1055–1063. https://doi.org/10.1007/s11071-013-0852-5
63. D. Yu, X. Y. Zhou, G. W. Wang, Q. Ding, T. Li, Y. Jia, Effects of chaotic activity and time delay on signal transmission in FitzHugh-Nagumo neuronal system, *Cognit. Neurodyn.*, **16** (2022), 887–897. https://doi.org/10.1007/s11571-021-09743-5
64. J. Ma, L. Huang, J. Tang, H. P. Ying, W. Y. Jin, Spiral wave death, breakup induced by ion channel poisoning on regular Hodgkin-Huxley neuronal networks, *Commun. Nonlinear Sci. Numer. Simul.*, **17** (2012), 4281–4293. https://doi.org/10.1016/j.cnsns.2012.03.009
65. D. M. Lombardo, W. J. Rappel, Chaotic tip trajectories of a single spiral wave in the presence of heterogeneities, *Phys. Rev. E*, **99** (2019), 062409. https://doi.org/10.1103/PhysRevE.99.062409
66. L. Lv, L. Ge, L. Gao, C. Han, C. Li, Synchronization transmission of spiral wave and turbulence in uncertain time-delay neuronal networks, *Phys. A*, **525** (2019), 64–71. https://doi.org/10.1016/j.physa.2019.03.054
67. J. Ma, C. N. Wang, J. Tang, Y. Jia, Eliminate spiral wave in excitable media by using a new feasible scheme, *Commun. Nonlinear Sci. Numer. Simul.*, **15** (2010), 1768–1776. https://doi.org/10.1016/j.cnsns.2009.07.013
68. J. Luo, T. C. Li, H. Zhang, Resonant drift of synchronized spiral waves in excitable media, *Phys. Rev. E*, **101** (2020), 032205. https://doi.org/10.1103/PhysRevE.101.032205
69. J. Luo, X. Zhang, J. Tang, Complex-periodic spiral waves induced by linearly polarized electric field in the excitable medium, *Int. J. Bifurcation Chaos*, **29** (2019), 1950071. https://doi.org/10.1142/S0218127419500718
70. J. Ma, B. Hu, C. N. Wang, W. Jin, Simulating the formation of spiral wave in the neuronal system, *Nonlinear Dyn.*, **73** (2013), 73–83. https://doi.org/10.1007/s11071-013-0767-1
71. J. Lober, H. Engel, Analytical approximations for spiral waves, *Chaos*, **23** (2013), 043135. https://doi.org/10.1063/1.4848576
72. J. Ma, L. Huang, H. P. Ying, Z. S. Pu, Detecting the breakup of spiral waves in small-world networks of neurons due to channel block, *Chin. Sci. Bull.*, **57** (2012), 2094–2101. https://doi.org/10.1007/s11434-012-5114-2
73. H. Kim, S. Shinomoto, Estimating nonstationary inputs from a single spike train based on a neuron model with adaptation, *Math. Biosci. Eng.*, **11** (2014), 49–62. https://doi.org/10.3934/mbe.2014.11.49
74. J. Ma, X. Song, J. Tang, C. Wang, Wave emitting and propagation induced by autapse in a forward feedback neuronal network, *Neurocomputing*, **167** (2015), 378–389. https://doi.org/10.1016/j.neucom.2015.04.056
75. L. Kostal, S. Shinomoto, Efficient information transfer by Poisson neurons, *Math. Biosci. Eng.*, **13** (2016), 509–520. https://doi.org/10.3934/mbe.2016004
76. J. Ma, C. N. Wang, W. Y. Jin, Y. Wu, Transition from spiral wave to target wave and other coherent structures in the networks of Hodgkin-Huxley neurons, *Appl. Math. Comput.*, **217** (2010), 3844–3852. https://doi.org/10.1016/j.amc.2010.09.043
77. M. Levakova, Effect of spontaneous activity on stimulus detection in a simple neuronal model, *Math. Biosci. Eng.*, **13** (2016), 551–568. https://doi.org/10.3934/mbe.2016007

78. M. Y. Ge, Y. Jia, Y. Xu, L. Lu, H. Wang, Y. Zhao, Wave propagation and synchronization induced by chemical autapse in chain Hindmarsh-Rose neural network, *Appl. Math. Comput.*, **352** (2019), 136–145. https://doi.org/10.1016/j.amc.2019.01.059
79. F. R. Mikkelsen, A model based rule for selecting spiking thresholds in neuron models, *Math. Biosci. Eng.*, **13** (2016), 569–578. https://doi.org/10.3934/mbe.2016008
80. D. Yu, G. W. Wang, T. Y. Li, Q. Ding, Y. Jia, Filtering properties of Hodgkin-Huxley neuron on different time-scale signals, *Commun. Nonlinear Sci. Numer. Simul.*, **117** (2023), 106894. https://doi.org/10.1016/j.cnsns.2022.106894
81. G. W. Wang, L. J. Yang, X. Zhan, A. Li, Y. Jia, Chaotic resonance in Izhikevich neural network motifs under electromagnetic induction, *Nonlinear Dyn.*, **107** (2022), 3945–3962. https://doi.org/10.1007/s11071-021-07150-3
82. G. W. Wang, Y. Wu, F. L. Xiao, Z. Ye, Y. Jia, Non-Gaussian noise and autapse-induced inverse stochastic resonance in bistable Izhikevich neural system under electromagnetic induction, *Phys. A*, **598** (2022), 127274. https://doi.org/10.1016/j.physa.2022.127274


AIMS Press